Journal of Sustainable Construction Materials and Technologies
Web page info: https://jscmt.yildiz.edu.tr
DOI: 10.47481/jscmt.1555157

JSCMT
Journal of Sustainable Construction Materials and Technologies

Research Article

A study on the influence of material gradient index on bending and stress responses of FGM rectangular plates using the Finite Element Method

Masihullah NOORI*, Ayça BİLGİN, Hamza DIALLO, Mohammad Omar AL ROUSAN, Ahmad Reshad NOORI

Department of Civil Engineering, İstanbul Gelişim University, İstanbul, Türkiye

ARTICLE INFO

Article history
Received: 19 June 2024
Revised: 30 August 2024
Accepted: 03 September 2024

Key words:
Bending, deflection, finite element method, FGM rectangular plate, stresses

ABSTRACT

Functionally graded materials (FGMs) are advanced materials designed to achieve specific property gradients. The unique characteristic of these materials—variations in spatial dimensions—allows for integrating the advantages of different materials within a single component, where a combination of properties, such as mechanical strength, thermal resistance, and others, is needed. This paper utilizes finite element analysis to examine the deflection and stress responses of FGM rectangular plates with different material gradient profiles. Various boundary conditions, including clamped, simply supported, and free edges in different configurations, are considered. The plates are subjected to uniformly distributed, sinusoidally distributed, and concentrated loads. The study investigates the effects of boundary and loading conditions, along with the impact of the material gradient, on the deflections and stress responses of FGM rectangular plates. The results indicate variations in deflection and stress values for different material gradients, under varying boundary and loading conditions.

Cite this article as: Noori, M., Bilgin, A., Diallo, H., Al Rousan, M. O., & Noori, A. R. (2024). A study on the influence of material gradient index on bending and stress responses of FGM rectangular plates using the Finite Element Method. *J Sustain Const Mater Technol*, 9(3), 239–254.

1. INTRODUCTION

Functionally graded materials (FGMs) are advanced composite materials with structural characteristics that provide customized mechanical, thermal, and chemical properties. The gradual variation in the composition or microstructure of these materials across spatial dimensions makes it possible to manipulate their properties based on practical needs [1]. Although FGMs have attracted significant attention owing to their potential applications in diverse engineering fields, including structural, aerospace, automotive, and biomedical engineering, future applications also demand materials that are readily available at reasonable costs and do not compromise environmental concerns [2].

Torelli et al. [3] comprehensively analyzed Functionally Graded Concrete (FGC), focusing on structural applications, design methods, and production procedures. Keeping in mind that the industrial production of cement, the critical constituent of concrete, accounts for approximately 5% of global human-made carbon emissions, they showed through their results that material savings of up to 40% are possible through the functional gradation of concrete. In their sustainability analysis, Chan et al. [4] investigated FGC made of recycled aggregates reinforced with fibers. They concluded that a reduction in the total volume of steel fibers, resulting from a decreased ratio of reinforced layer height to total height, minimized the total embodied CO2 and cost of concrete.

***Corresponding author.**
*E-mail address: masihullahnoori12@gmail.com

Sustaining energy demands for the current generation can pose significant environmental challenges for upcoming generations. Although progress in this field seems gradual, it aligns with innovations in materials, equipment, and environmental considerations [5]. The concept of FGMs dates back to the late 20th century, with initial conceptualizations emerging during a space plane project in Japan in the 1980s [6]. Advancements in material processing techniques during the 1990s and early 2000s, such as powder metallurgy and sol-gel methods, facilitated the manufacturing of FGM structures with greater control over material properties. Today, producing graded structures can be considered the next step in the development of composite materials [7].

Academic researchers have conducted comprehensive studies on the behavior of structural elements composed of FGMs in different applications, illustrating their mechanical, thermal, and chemical responses. Chaabani et al. [8] studied the buckling and post-buckling behavior of porous FGM plates using High Order Continuation based on the Asymptotic Numerical Method in conjunction with the Finite Element Method (FEM) to model the nonlinear behavior of a Porous Functionally Graded Material (PFGM) plate. Several plates with different porosity distributions under various types of transverse loads were analyzed, and they concluded that an increase in the porosity coefficient of PFGM plates causes more significant deflections, thereby diminishing plate stiffness and reducing critical buckling loads.

Moita et al. [9] investigated higher-order finite element models for the static linear and nonlinear response of FGM plate-shell structures. Their study revealed that the gradient index can determine the mechanical behavior of FGM plates. They also highlighted the influence of high temperatures on the predictability of these responses. Afzali et al. [10] conducted a study to investigate the thermal buckling response of FGM plates with temperature-dependent properties. Their findings revealed that using the actual temperature distribution instead of assumed ones can lead to more precise results in thermal buckling analysis. Kazemzadeh-Parsi et al. [11] analyzed the thermoelasticity of FGMs using Proper Generalized Decomposition (PGD), primarily focusing on material gradation in one, two, and three directions. They reduced high-dimensional problems to one-dimensional problems, contributing to the simplicity of the solution and design procedure.

Kargarnovin et al. [12] investigated the thermal buckling behavior of FGM rectangular plates using the Classical Plate Theory (CPT) and the Galerkin method. They concluded that plate geometry and material properties can influence the critical buckling temperature. Saad and Hadji [13] studied different parameters affecting the critical buckling temperature of thick FGM plates. They presented numerical results derived from thermal buckling analyses on FGM plates subjected to uniform, linear, and non-linear thermal loading conditions. Using the four-variable higher-order shear Deformation Theory (HSDT), they underscored the validity of the proposed shear theory in resolving the buckling behavior of PFGM plates under varied thermal loading conditions.

Slimani et al. [14] used the seemingly 3D refined HSDT to investigate the static bending with two distinct types of porosity dispersal in FGM plates. The results showed that the E-FGM (exponential function) yielded larger deflection values, normal stresses, and shear stresses than the P-FGM (power-law function). Rebai et al. [15] investigated an analytical approach based on micromechanical models to analyze the static deflection behavior of sandwich FGM plates subjected to thermal loads. A comparative outcome stated that while various micromechanical models affect the deflection behavior, their overall impact on the deflection behavior is relatively small.

Hamza and Bouderba [16], using an efficient and straightforward refined plate theory, analyzed the buckling of FGM plates subjected to different load conditions. They explored the effects of uniaxial and biaxial compression loads, alongside simply supported boundary conditions, on rectangular FGM plates. Their results confirmed that the application of uniaxial and biaxial compressive loads, coupled with transverse shear loading, stabilizes the shear buckling phenomenon of FGM plates subjected to combined shear and directional loading.

Hong [17] studied static bending and free vibration analysis of bidirectional FGM plates using FEM and third-order shear deformation theory. He concluded that increased deformation and load intensity applied to the structure leads to conflicts arising from linear and nonlinear problems. Talha and Singh [18] conducted free vibration and static analysis of square and rectangular FGM plates based on HSDT in conjunction with FEM. A special modification was made to the transverse displacement. An increase in frequency parameter was observed and confirmed, resulting from increased plate aspect ratio and smaller side-to-thickness ratio.

Singh and Gupta [19] used HSDT to investigate the effects of porosity integration and geometric flaws on the vibrational frequency of sandwich functionally graded material (SFGM) plates under both usual and unusual boundary conditions. They found that due to a reduction in metallic content, the non-dimensional frequency parameter (NDFP) decreases as the volume fraction index (n) decreases from metal to ceramic, reducing the overall stiffness of the SFGM plate. While HSDT can be more accurate than the four-variable shear deformation theory (FVSDT), FVSDT strikes a balance between accuracy and computational efficiency, making it suitable for various applications involving moderate thicknesses and shear deformation effects. Alghanmi and Aljaghthami [20] utilized FVSDT to investigate the effects of nonuniform heterogeneous parameters, aspect ratios, side-to-thickness ratios, and changing porosities on the sandwich plates' static bending behavior. They found that higher porosity leads to greater deflections. This may also be known as the elasticity modulus deterioration resulting from excessive porosities, which causes the plate's bending stiffness to decline. Because the plate bending stiffness is reduced at greater side-to-thickness and lower aspect ratio, the center deflection is amplified even more.

Nguyen et al. [21] investigated the buckling properties of variable thickness functionally graded porous (FGP) plates with sinusoidal porosity distribution. They achieved this by integrating ES-MITC3 with First Order Shear Deformation Theory (FSDT). They discovered that since the ES-MITC3 is built on traditional triangular elements, meshing elements with complicated geometries is simpler. The FGP plate rigidity decreases with a rise in the power-law index, which lowers the critical load. Elkafrawy et al. [22] investigated the elastic buckling of FGM thin plates with circular, square, and diamond-shaped openings using FEM. Their analysis revealed that enlarging the opening and adjusting the aspect ratio reduced the critical buckling load for the FGM plate.

Alashkar et al. [23] studied the buckling analysis of FGM thin plates with various circular cutout arrangements using FEM. They concluded that the critical buckling load increases as the plate thickness decreases and the circular cutout diameter increases. In a separate study, they investigated the elastic buckling characteristic of skew FGM thin plates with a circular opening using FEM. They found that the critical buckling load also increases as the skew angle rises. Furthermore, the critical buckling load declines as the opening moves from the plate's border toward its center [24].

Kumar et al. [25] presented the modified Radial Basis Function (RBF)-based mesh-free method for the initial buckling analysis of elastically supported rectangular FGM plates subjected to various in-plane loading conditions. A thin plate spline RBF method was implemented. They found that the critical buckling load generally decreases as the aspect ratio increases for all loading arrangements. Shehab et al. [26] investigated the free vibration analysis of intact and cracked FGM plates using experimental and numerical methods. The results showed that when the FGM gradient index is less than 3, it significantly affects the plate's natural frequency, while higher gradient indexes have no significant effect on both cracked and intact plates.

Hu et al. [27] proposed the Symplectic Superposition Method (SSM) as an analytical method to solve the free vibration problem of non-Lévy type porous FGM rectangular plates. Their study highlighted that SSM doesn't need pre-defined solution forms, paving the way for obtaining rapidly convergent frequency results with high accuracy. Peng et al. [28] found that the fundamental frequency of the stiffened FGM plates resting on the Winkler foundation varies with variations in the power-law exponent. Lim et al. [29] investigated a sophisticated, multilayered modeling approach, likely based on FEM, for the static analysis of porous FGM cooling plates with cutouts. By considering various conventional and unconventional boundary conditions, they discovered that the location of clamped edges significantly impacts the deflection, with a specific configuration (BC3) exhibiting the lowest deflection. Ramu and Mohanty [30] coded an FGM plate program in MATLAB to determine its natural frequencies and mode shapes using FEM. It was observed that increasing the power-law index value (n) reduced the first five natural frequencies under various boundary conditions in their study.

In their study, Srivastava et al. [31] analyzed Radial Basis Functions (RBFs) with modified radial distance for the vibration analysis of FGM rectangular plates using HSDT. Their findings showed that increasing grading and porosity indexes causes a decrease in normalized natural frequency. Kumar [32], in his free transverse vibration analysis of a thin isotropic FG rectangular plate with porosity effects based on CPT, concluded that the frequencies of isotropic simply supported plates are proportional to those of merely supported homogeneous isotropic plates. Kumaravelan [33], in his thesis, studied the axisymmetric bending of FGM circular plates under uniformly distributed transverse mechanical, thermal, and combined mechanical-thermal loads using the Element Free Galerkin (EFG) method. He concluded that adding a metal or ceramic plate to one face of a tapered FGM plate decreases the induced stresses. Therefore, in cases where the FGM plate does not have sufficient strength for a particular application, a metal or ceramic plate can be bonded to the FGM plate.

Smaine et al. [34] investigated the volumetric proportion of the FGM concept in the Fiber-Matrix mixing laws in UD composites using the ABAQUS calculation code and FEM. They noticed that the suggested graded composite exhibited overcapacity of resistance as indicated by the grading index (n) or their locations. The fibers C1 and C2 contributed to optimizing this capacity. Asemi and Salami [35] extended a numerical approach for the low-velocity impact analysis of rectangular FGM plates based on the 3D theory of elasticity. They concluded that applying 3D-graded elements to analyze the plates eliminates the discontinuities in the stress distribution that are present in conventional FE results. Rani et al. [36] developed the Extended Finite Element Method (XFEM) and the level set method for modeling and analyzing stresses around rounded rectangular inclusions enclosed with an FGM layer. They demonstrated that the FGM layer significantly reduces the stress concentration and identified optimal FGM properties for minimizing it.

Yildirim [37] investigated hydrogen-induced stresses in FGM circular members using the two-dimensional theory of elasticity. Through his simple and efficient procedure, he concluded that radial stress is more affected by the material model selection than hoop stress. Feri et al. [38] studied the 3D bending behavior of an intelligent plate consisting of a viscoelastic FGM layer sandwiched between piezoelectric layers under electric field and pressure. The analysis used a state-space technique and Fourier series expansion to solve the governing equations in the Laplace domain. Based on the numerical results, it was demonstrated that the viscoelastic properties strongly affect the bending behavior of the FGM plate.

Bendenia et al. [39] studied the static and free vibration behavior of nanocomposite sandwich plates reinforced with carbon nanotubes. It was found that functionally graded carbon nanotube face sheet-reinforced sandwich plates have high resistance against deflections compared to other reinforcements. Several other structural elements, such as beams, arches, columns, domes, etc., composed of functionally

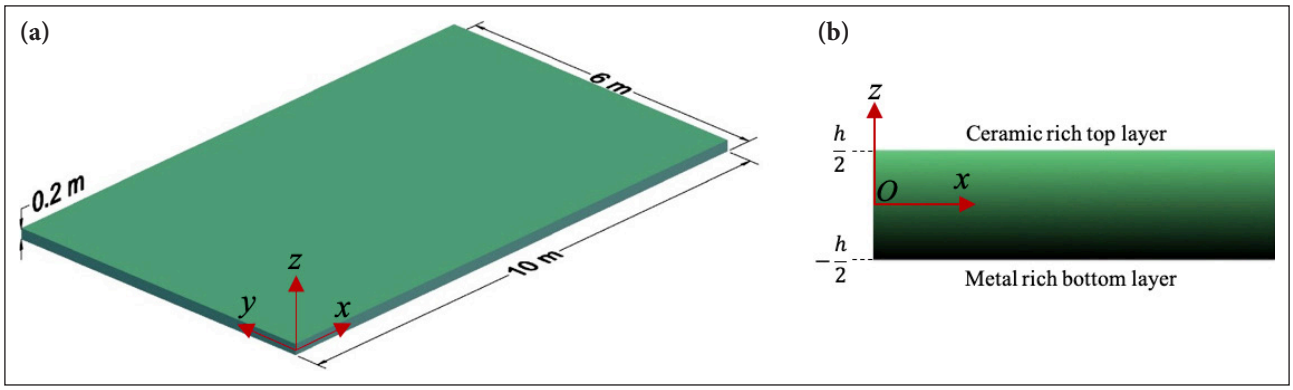

Figure 1. **(a)** FGM rectangular plate; **(b)** Cross section of FGM rectangular plate.

graded materials, have also been investigated by researchers, shedding light on various behavioral aspects of FGMs in diverse applications [40–48]. Researchers have utilized a wide range of analytical models to solve these problems.

Menasria et al. [49] ensured the zero-shear stresses at the free surfaces of functionally graded sandwich plates without introducing any correction factor by proposing a refined shear deformation theory with fewer unknowns. Through verification studies, Rabhi et al. [50] confirmed that their three-unknown shear deformation theory is comparable with other higher-order shear deformation theories in solving problems related to the buckling and vibration responses of exponentially graded sandwich plates.

Matouk et al. [51] investigated the free vibration responses of functionally graded nano-beams using integral Timoshenko beam theory. Their model has three variable unknowns and requires the introduction of a shear correction factor due to uniformly varied shear stress in the thickness direction. In finite element analysis, mesh density is an essential concept that closely relates to the accuracy of finite element models while directly determining their complexity level.

Hassan and Kurgan [52] modeled and analyzed the buckling of rectangular plates using the ANSYS software package, emphasizing selecting an appropriate number of elements in FEM. A large number of elements leads to more computational time without a significant gain in accuracy, while too few elements can produce incorrect solutions. Extensive research studies have been conducted to explore the impact of mesh refinement in both static and dynamic analyses. A consensus is present among all the conducted studies that the fineness of the mesh can significantly influence the obtained results [53, 54].

This paper analyzes FGM plates with various material gradients in the thickness direction using the finite element package program ANSYS Mechanical APDL [55]. The effects of material gradients, boundary conditions, and load types on the deflection and stress responses of FGM plates are investigated. The study aims to illustrate how increasing the power-law index, which introduces more steel constituents into the mix, can affect the bending and stress responses of FGM plates. Additionally, the influence of constraints at the edges of the plates on bending and stress formation within the FGM plates is studied. A convergence study also discusses the optimal number of layers and mesh density for discretizing these plates.

2. MATERIALS AND METHODS

In this paper, an FGM rectangular plate, as shown in Figure 1, with various types of boundary conditions subjected to three distinct load forms, is studied using the FEM. For this study, the dimensions of the rectangular plate were arbitrarily selected without any specific rationale. The length and width of the plate are considered to be 10 and 6 meters with a thickness (h) of 20 centimeters. The Cartesian coordinate system $Oxyz$, where O is the origin of the coordinate system, is located at the left corner of the mid-plane of the plate, in which x, y, and z are the planer in-plane and vertical out-of-plane coordinates, respectively. Functionally gradation of materials in the thickness direction of the plate is shown in Figure 1.

Young's modulus of elasticity E is assumed to be a function of spatial coordinate z in the thickness direction and can vary linearly or non-linearly. Thus, the material properties of the FGM plate can be obtained by the rule of mixture as follows [56]:

$$V_c+V_m=1 \quad (1)$$

$$E(z)=E_c V_c+E_m V_m=(E_c-E_m)\, V_c+E_m \quad (2)$$

V_c and V_m are volume fractions, and E_c and E_m are Young's modulus of elasticity for the FGM ceramic and metal components, respectively. The volume fraction of ceramic as a function of the thickness z coordinate can be determined by a power-law function [56]:

$$V_c = \left(\frac{1}{2}+\frac{z}{h}\right)^n,\ n \geq 0 \quad (3)$$

Where z is the dimensionless coordinate in the thickness direction, h is the total thickness of the plate, and n is the power-law index, which indicates the material variation profile in the thickness direction. At the top ceramic-rich layer ($z=h/2$), $n=0$ leads Eq. 2 to $E(z)=E_c$, and at the bottom metal-rich layer ($z=-h/2$), $n=\infty$ leads Eq. 2 to $E(z)=E_m$. Delale and Erdogan investigated the effect of Poisson's ratio on the deformation of plates [57]. They concluded that Poisson's ratio had a much lower impact on deformation than Young's modulus. Thus, the Pois-

Table 1. Material properties

Material	Young's modulus (GPa)	Poisson ratio
Ceramic - Alumina (Al_2O_3)	380	0.3
Steel	200	0.3

son's ratio of the plate is assumed to be constant. Alumina and steel are considered ceramic and metal materials in this study, and their properties are presented in Table 1. Variations of Young's modulus of elasticity in the thickness direction of the plate for different power-law indexes (n) are shown in Figure 2.

The plates were analyzed using the finite element package program ANSYS Mechanical APDL, and a 3D element SHELL281 [58] was selected for discretization. SHELL281 is appropriate for the analysis of thin to moderately thick shell structures. This element is based on first-order shear deformation theory, which governs the accuracy of modeling composite or sandwich structures. It is also well-suited for linear applications involving large rotations and/or strain nonlinearities. This finite element has eight nodes, each with six degrees of freedom: translations along the x, y, and z axes and rotations around the x, y, and z axes. The geometric configuration of SHELL281 is shown in Figure 3.

Shape functions of 3D 8-node SHELL281 element are presented through Eqs. (4–9) [58].

$$u = \frac{1}{4}\left(u_I(1-s)(1-t)(-s-t-1) + u_J(1+s)(1-t)(s-t-1) + u_K(1+s)(1+t)(s+t-1) + u_L(1-s)(1+t)(-s+t-1)\right) + \frac{1}{2}\left(u_M(1-s^2)(1-t) + u_N(1+s)(1-t^2) + u_O(1-s^2)(1+t) + u_P(1-s)(1-t^2)\right) \quad (4)$$

$$v = \frac{1}{4}\left(v_I(1-s)(1-t)(-s-t-1) + v_J(1+s)(1-t)(s-t-1) + v_K(1+s)(1+t)(s+t-1) + v_L(1-s)(1+t)(-s+t-1)\right) + \frac{1}{2}\left(v_M(1-s^2)(1-t) + v_N(1+s)(1-t^2) + v_O(1-s^2)(1+t) + v_P(1-s)(1-t^2)\right) \quad (5)$$

$$w = \frac{1}{4}\left(w_I(1-s)(1-t)(-s-t-1) + w_J(1+s)(1-t)(s-t-1) + w_K(1+s)(1+t)(s+t-1) + w_L(1-s)(1+t)(-s+t-1)\right) + \frac{1}{2}\left(w_M(1-s^2)(1-t) + w_N(1+s)(1-t^2) + w_O(1-s^2)(1+t) + w_P(1-s)(1-t^2)\right) \quad (6)$$

$$\theta_x = \frac{1}{4}\left(\theta_{x_I}(1-s)(1-t)(-s-t-1) + \theta_{x_J}(1+s)(1-t)(s-t-1) + \theta_{x_K}(1+s)(1+t)(s+t-1) + \theta_{x_L}(1-s)(1+t)(-s+t-1)\right) + \frac{1}{2}\left(\theta_{x_M}(1-s^2)(1-t) + \theta_{x_N}(1+s)(1-t^2) + \theta_{x_O}(1-s^2)(1+t) + \theta_{x_P}(1-s)(1-t^2)\right) \quad (7)$$

$$\theta_y = \frac{1}{4}\left(\theta_{y_I}(1-s)(1-t)(-s-t-1) + \theta_{y_J}(1+s)(1-t)(s-t-1) + \theta_{y_K}(1+s)(1+t)(s+t-1) + \theta_{y_L}(1-s)(1+t)(-s+t-1)\right) + \frac{1}{2}\left(\theta_{y_M}(1-s^2)(1-t) + \theta_{y_N}(1+s)(1-t^2) + \theta_{y_O}(1-s^2)(1+t) + \theta_{y_P}(1-s)(1-t^2)\right) \quad (8)$$

$$\theta_z = \frac{1}{4}\left(\theta_{z_I}(1-s)(1-t)(-s-t-1) + \theta_{z_J}(1+s)(1-t)(s-t-1) + \theta_{z_K}(1+s)(1+t)(s+t-1) + \theta_{z_L}(1-s)(1+t)(-s+t-1)\right) + \frac{1}{2}\left(\theta_{z_M}(1-s^2)(1-t) + \theta_{z_N}(1+s)(1-t^2) + \theta_{z_O}(1-s^2)(1+t) + \theta_{z_P}(1-s)(1-t^2)\right) \quad (9)$$

Where u, v, and w are displacement components, θ_x, θ_y, and θ_z are rotation components in x, y, and z directions, respectively, and s and t are local coordinates within the finite element.

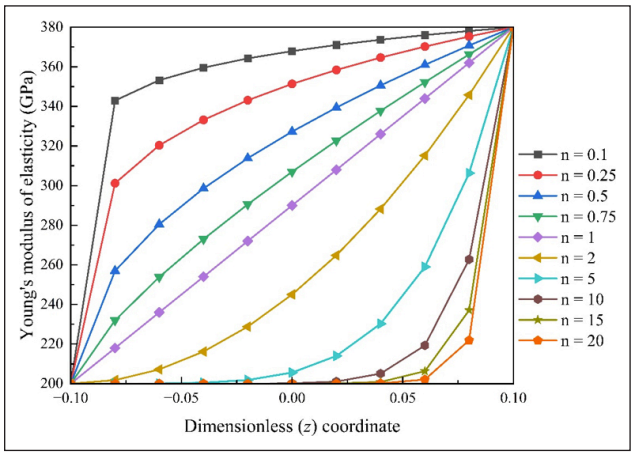

Figure 2. Young's modulus of elasticity in the thickness direction for different values of n.

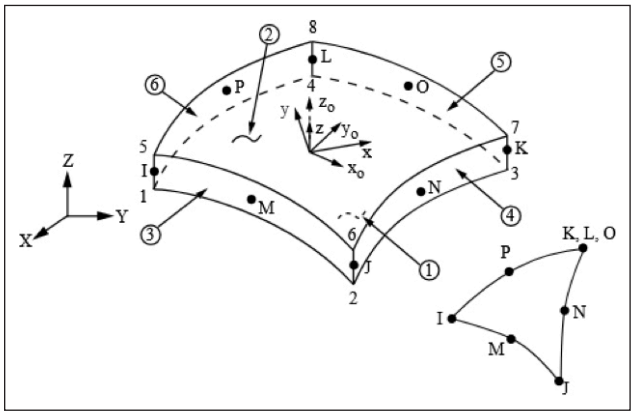

Figure 3. SHELL281 geometry [58].

2.1. Convergence Study

A convergence study was conducted to model the FGM plates in ANSYS Mechanical APDL and determine the appropriate number of layers and mesh size for discretization. Singha et al. [56] used a high-precision plate bending element based on first-order shear deformation theory to analyze the deflection and stresses of FGM plates under distributed transverse load. In their study, the formulation realistically accounted for the neutral surface position and the shear correction factors. Different boundary conditions with uniformly and lateral sinusoidal distributed loads were examined. For this study, only the results obtained in their research for the non-dimensional central displacement of clamped thin square alumina/aluminum FGM plates with power law indexes 0, 1, 2, 3, 4, 5, 10, and ∞ under uniformly distributed load were selected and compared with the results of the present study. The results of the present study and their study exhibit substantial agreement, affirming the reliability of the findings and validating the methodology used in this research. Comparisons of non-dimensional central displacement values of FGM plates with varying numbers of layers and mesh sizes are tabulated in Table 2 and Table 3, respectively.

As presented in Table 2, one layer is qualifying enough to obtain reliable results in the case of isotropic homoge-

Table 2. Non-dimensional central displacement of FGM plates with varying number of layers

Number of layers	Power-law index (n)							
	0	1	2	3	4	5	10	∞
1	0.001267	–	–	–	–	–	–	0.006890
11	–	0.002638	0.003229	0.003480	0.003584	0.003654	0.003828	–
21	–	0.002589	0.003243	0.003515	0.003654	0.003758	0.004002	–
31	–	0.002575	0.003250	0.003549	0.003689	0.003793	0.004071	–
41	–	0.002565	0.003250	0.003549	0.003689	0.003793	0.004106	–
51	–	0.002561	0.003254	0.003549	0.003723	0.003793	0.004141	–
61	–	0.002558	0.003254	0.003549	0.003723	0.003828	0.004141	–
71	–	0.002558	0.003254	0.003549	0.003723	0.003828	0.004176	–
81	–	0.002554	0.003257	0.003584	0.003723	0.003828	0.004176	–
91	–	0.002554	0.003257	0.003584	0.003723	0.003828	0.004176	–
101	–	0.002551	0.003257	0.003584	0.003723	0.003828	0.004176	–
201	–	0.002547	0.003257	0.003584	0.003723	0.003828	0.004211	–
Singha et al. [56]	0.001267	0.002542	0.003258	0.003580	0.003746	0.003854	0.004233	0.006881

Table 3. Non-dimensional central displacement of FGM plates with different mesh sizes

Power-law index (n)	Mesh sizes						Singha et al. [56]
	5 x 5	10 x 10	20 x 20	30 x 30	40 x 40	50 x 50	
0	0.000936	0.001267	0.001267	0.001267	0.001267	0.001267	0.001267
1	0.001837	0.002544	0.002547	0.002547	0.002547	0.002547	0.002542
2	0.002380	0.003250	0.003257	0.003257	0.003257	0.003257	0.003258
3	0.002666	0.003584	0.003584	0.003584	0.003584	0.003584	0.003580
4	0.002822	0.003723	0.003723	0.003723	0.003723	0.003723	0.003746
5	0.002930	0.003828	0.003828	0.003828	0.003828	0.003828	0.003854
10	0.003243	0.004211	0.004211	0.004211	0.004211	0.004211	0.004233
∞	0.005081	0.006855	0.006890	0.006890	0.006890	0.006890	0.006881

Table 4. Transitional and rotational restraints of supports

Type of support	Restraints
Clamped (C)	Ux = Uy = Uz = Rotx = Roty = Rotz = 0
Simply supported (S)	At x = 0 and 10, Uy = Uz = 0, At y = 0 and 6, Ux = Uz = 0
Free (F)	–

neous thin plates. In the FGM plates, the results converged as the number of layers in the thickness direction was increased. No significant change was observed in non-dimensional central displacement values of FGM plates after adding more than 201 layers. In Table 3, the values of non-dimensional central displacements for all plates were the same for finer meshes after 20 x 20. Although the non-dimensional central displacements of an isotropic homogeneous ceramic plate are the same after a 10 x 10 mesh size, in the case of an isotropic homogeneous metal plate, the results converged after a 20 x 20 mesh size. These findings suggest the sufficiency of 201 layers and 20 x 20 mesh size in solving thin to moderately thick FGM plates, yielding acceptable results while minimizing computational time. They also indicate a high degree of consistency and validation across both studies. The modeling and analyzing procedure of the present study is shown through a flowchart in Figure 4.

3. RESULTS AND DISCUSSION

This paper investigates deflections and stress responses of FGM plates with different boundary conditions subjected to three types of loads. All FGM plates have 201 layers in the thickness direction, with each layer having its distinct material properties calculated by using Eq. 2. The variations of these material properties are based on the considered power-law indexes (0, 0.1, 0.25, 0.5, 0.75, 1, 2, 5, 10, 15, and 20). A mesh size of 20 x 20 is used for discretization. Seven different boundary conditions are taken into account. The

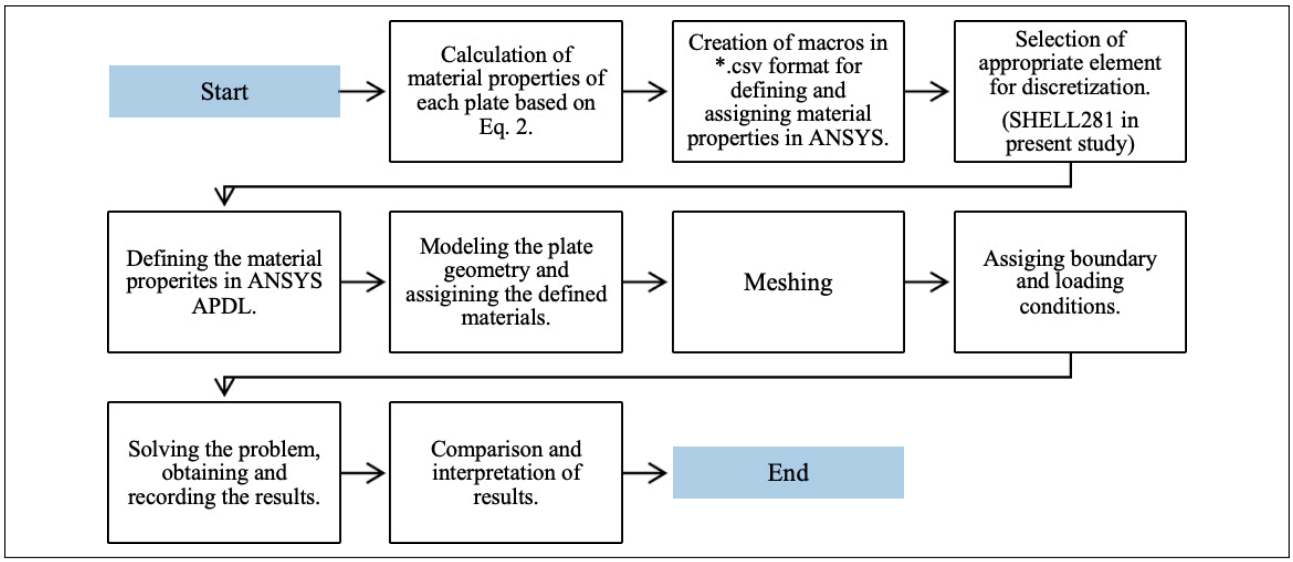

Figure 4. Modeling and analyzing procedure.

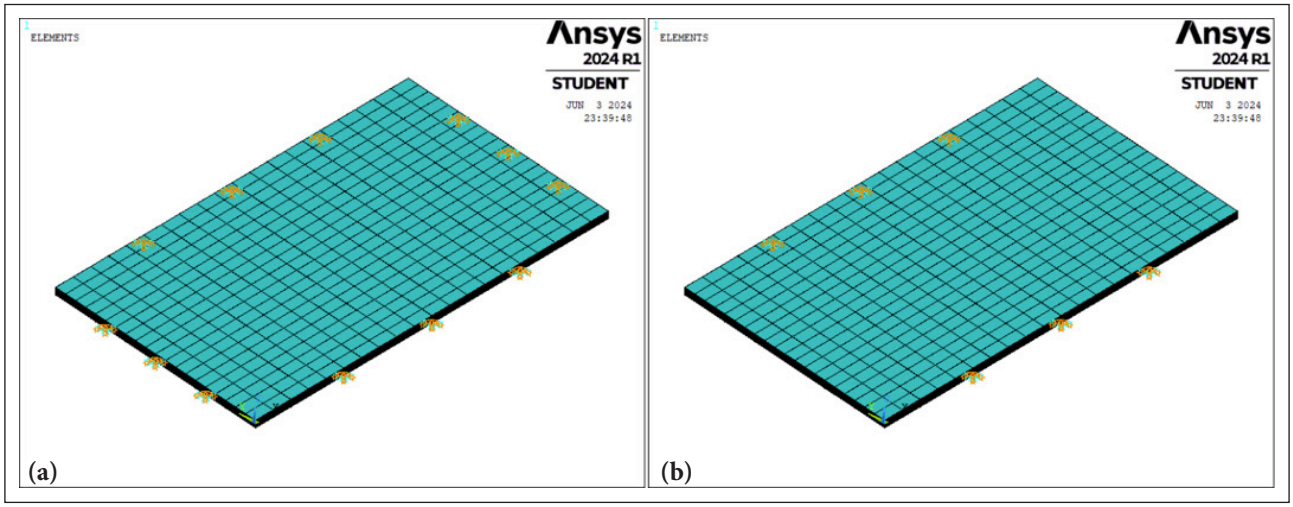

Figure 5. Meshed FGM rectangular plates with **(a)** CCCC and **(b)** CCFF boundary conditions.

transitional and rotational restraints of the supports are presented in Table 4. The configuration of the boundary conditions is such that from the left side, the first two letters represent the bottom and top, and the last two letters represent the left and right edges of the plate. Figure 5 shows meshed FGM rectangular plates with CCCC and CCFF boundary conditions.

10 FGM plates with distinct material properties are modeled and analyzed with seven boundary conditions and three different load types. A concentrated point load is assigned at the center point of the top ceramic-rich face. Uniformly and sinusoidal distributed loads were assigned on the top ceramic-rich face of the plate. The function of sinusoidal load is presented in Eq. 10.

$$P = p_0 \sin\left(\frac{\pi x}{a}\right) \sin\left(\frac{\pi y}{b}\right) \tag{10}$$

Where P is the sinusoidal load, a and b represent the length and width of the plate, respectively, and p_0 The magnitude of uniformly distributed load is assumed to be *10 kN* per square meter. It is worth mentioning that there is no specific reason for assigning this magnitude of load on the plate, and it is selected completely arbitrarily for this study. Maximum deflections of different FGM plates under uniformly distributed load, sinusoidal distributed load, and concentrated point loads with various boundary conditions are obtained and tabulated in Tables 5–7 and are compared in Figures 6–8, respectively. The results corresponding to the isotropic homogeneous ceramic and metal plates are included only in the tables to provide a wider scope of comparison.

As is evident from Figures 6–8, the smallest deflections were obtained in the case of sinusoidal and uniformly distributed loads, respectively, while the highest deflections were observed when the plates were subjected to concentrated point load. This is a result of the nature of the loading. Sinusoidal load varies smoothly and gradually across the plate, peaking at the center and reducing towards the edges in an illustrative manner, which paves the way for a more evenly spread out of stress and strain over the surface of the plate. This smooth distribution causes minimum local stress concentration and deflection. Uniformly distributed

Table 5. Maximum deflections (m) of isotropic homogeneous and FGM rectangular plates under uniformly distributed load

Power-law index (n)	Boundary conditions						
	CCCC	SSSS	CCSS	CSCS	CCCF	SSSF	CCFF
0	0.000112	0.000412	0.000121	0.000206	0.000139	0.000702	0.000139
0.1	0.000119	0.000439	0.000128	0.000220	0.000148	0.000747	0.000148
0.25	0.000127	0.000469	0.000137	0.000235	0.000159	0.000800	0.000158
0.5	0.000138	0.000509	0.000149	0.000255	0.000172	0.000868	0.000172
0.75	0.000145	0.000538	0.000157	0.000269	0.000182	0.000916	0.000181
1	0.000151	0.000558	0.000163	0.000279	0.000188	0.000950	0.000188
2	0.000162	0.000598	0.000175	0.000300	0.000202	0.001019	0.000202
5	0.000173	0.000638	0.000187	0.000320	0.000216	0.001086	0.000215
10	0.000182	0.000672	0.000197	0.000337	0.000227	0.001144	0.000226
15	0.000188	0.000693	0.000203	0.000347	0.000234	0.001180	0.000234
20	0.000192	0.000708	0.000207	0.000354	0.000239	0.001205	0.000238
∞	0.000212	0.000783	0.000229	0.000392	0.000265	0.001333	0.000264

Table 6. Maximum deflections (m) of isotropic homogeneous and FGM rectangular plates under sinusoidal distributed load

Power-law index (n)	Boundary conditions						
	CCCC	SSSS	CCSS	CSCS	CCCF	SSSF	CCFF
0	0.0000819	0.000263	0.0000863	0.000139	0.0000844	0.000306	0.0000867
0.1	0.0000872	0.000280	0.0000919	0.000148	0.0000899	0.000326	0.0000923
0.25	0.0000934	0.000299	0.0000983	0.000158	0.0000962	0.000349	0.0000988
0.5	0.0001010	0.000325	0.0001070	0.000171	0.0001040	0.000379	0.0001070
0.75	0.0001070	0.000343	0.0001130	0.000181	0.0001100	0.000400	0.0001130
1	0.0001110	0.000355	0.0001170	0.000188	0.0001140	0.000415	0.0001170
2	0.0001190	0.000381	0.0001250	0.000201	0.0001230	0.000445	0.0001260
5	0.0001270	0.000406	0.0001340	0.000215	0.0001310	0.000474	0.0001340
10	0.0001340	0.000428	0.0001410	0.000226	0.0001380	0.000499	0.0001410
15	0.0001380	0.000442	0.0001450	0.000233	0.0001420	0.000515	0.0001460
20	0.0001410	0.000451	0.0001480	0.000238	0.0001450	0.000526	0.0001490
∞	0.0001560	0.000499	0.0001640	0.000264	0.0001600	0.000582	0.0001650

Table 7. Maximum deflections (m) of isotropic homogeneous and FGM rectangular plates under concentrated point load

Power-law index (n)	Boundary conditions						
	CCCC	SSSS	CCSS	CSCS	CCCF	SSSF	CCFF
0	0.000576	0.001269	0.000585	0.000787	0.000581	0.001347	0.000585
0.1	0.000613	0.001351	0.000662	0.000838	0.000618	0.001434	0.000623
0.25	0.000656	0.001445	0.000666	0.000896	0.000661	0.001534	0.000666
0.5	0.000712	0.001568	0.000722	0.000972	0.000717	0.001665	0.000723
0.75	0.000751	0.001655	0.000762	0.001026	0.000757	0.001757	0.000763
1	0.000779	0.001717	0.000791	0.001065	0.000786	0.001823	0.000792
2	0.000838	0.001844	0.000850	0.001144	0.000844	0.001957	0.000851
5	0.000895	0.001967	0.000908	0.001221	0.000902	0.002087	0.000909
10	0.000943	0.002072	0.000957	0.001286	0.000950	0.002198	0.000957
15	0.000972	0.002137	0.000987	0.001326	0.000980	0.002266	0.000987
20	0.000992	0.002181	0.001007	0.001353	0.001000	0.002314	0.001007
∞	0.001095	0.002411	0.001112	0.001495	0.001104	0.002559	0.001112

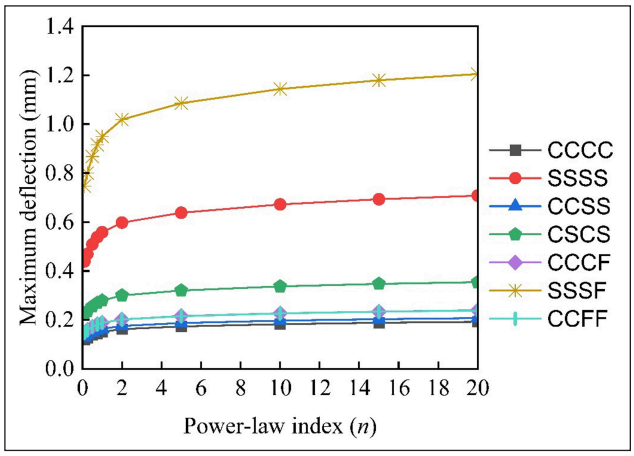

Figure 6. Maximum deflections of FGM rectangular plates under uniformly distributed load.

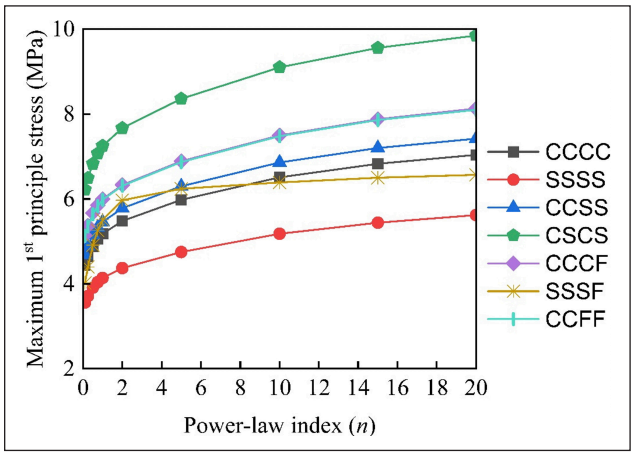

Figure 9. Maximum 1st principle stresses of FGM rectangular plates under uniformly distributed load.

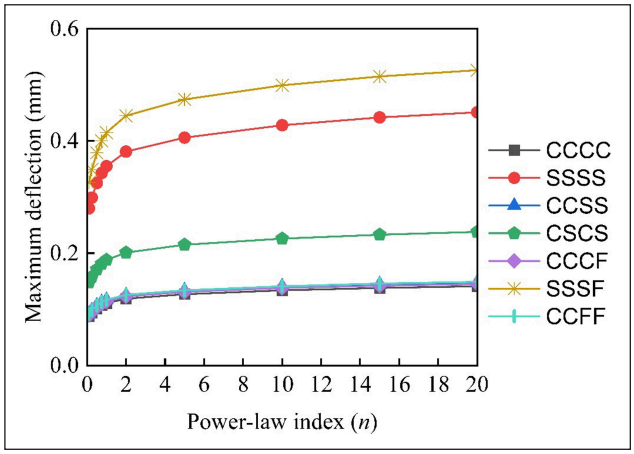

Figure 7. Maximum deflections of FGM rectangular plates under sinusoidal distributed load.

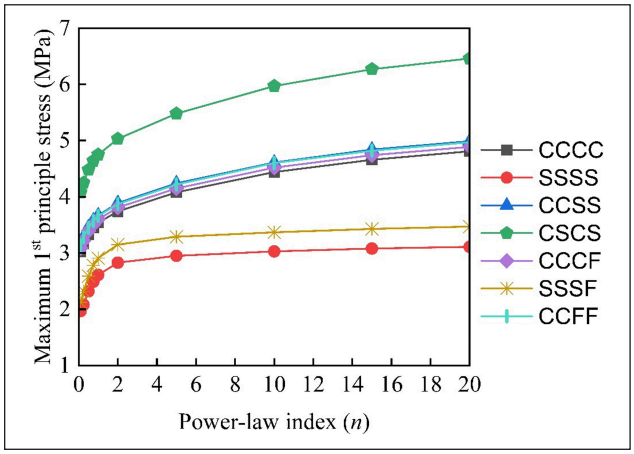

Figure 10. Maximum 1st principle stresses of FGM rectangular plates under sinusoidal distributed load.

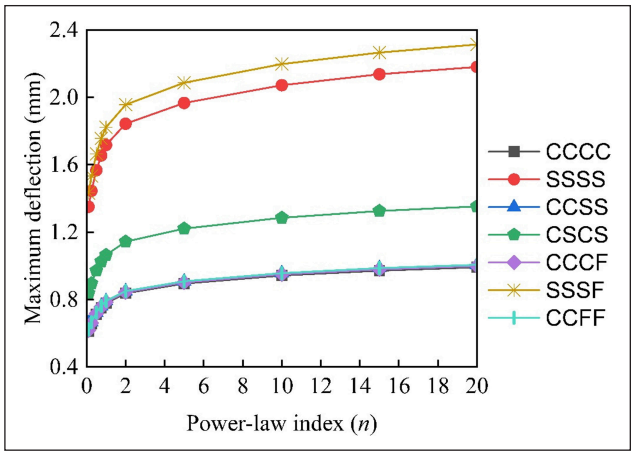

Figure 8. Maximum deflections of FGM rectangular plates under concentrated point load.

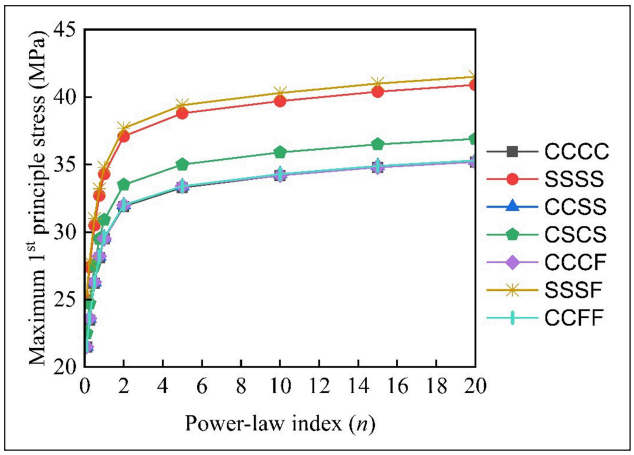

Figure 11. Maximum 1st principle stresses of FGM rectangular plates under concentrated point load.

load resulted in slightly higher deflections due to the constant magnitude over the entire face of the plate. Point Load, on the other hand, exhibited the highest deflections in FGM plates due to high-stress concentration at the point of application. The effect of boundary conditions on the deflection values of the FGM plates can be observed, too. In all three cases, SSSF, SSSS, and CSCS-type boundary conditions resulted in higher deflections than the others. Plates with SSSF boundary conditions have higher deflections because the free edge allows maximum movement, and simply support-

Table 8. Maximum 1st principle stresses (MPa) of isotropic homogeneous and FGM rectangular plates under uniformly distributed load

Power-law index (n)	Boundary conditions						
	CCCC	SSSS	CCSS	CSCS	CCCF	SSSF	CCFF
0	4.27	4.91	4.50	5.98	4.94	7.01	4.92
0.1	4.44	3.56	4.68	6.22	5.14	4.02	5.13
0.25	4.64	3.71	4.89	6.49	5.37	4.40	5.35
0.5	4.88	3.91	5.15	6.83	5.67	4.91	5.64
0.75	5.06	4.04	5.33	7.07	5.85	5.26	5.83
1	5.18	4.14	5.46	7.25	6.00	5.51	5.98
2	5.48	4.37	5.78	7.67	6.33	5.97	6.31
5	5.98	4.75	6.30	8.36	6.89	6.24	6.87
10	6.51	5.18	6.86	9.10	7.50	6.39	7.48
15	6.83	5.44	7.20	9.56	7.88	6.50	7.86
20	7.04	5.62	7.42	9.85	8.13	6.57	8.10
∞	4.27	4.91	4.50	5.98	4.94	7.01	4.92

Table 9. Maximum 1st principle stresses (MPa) of isotropic homogeneous and FGM rectangular plates under sinusoidal distributed load

Power-law index (n)	Boundary conditions						
	CCCC	SSSS	CCSS	CSCS	CCCF	SSSF	CCFF
0	2.92	3.32	3.03	3.92	2.97	3.70	3.02
0.1	3.03	1.97	3.15	4.08	3.09	2.12	3.14
0.25	3.17	2.08	3.29	4.25	3.22	2.32	3.28
0.5	3.33	2.32	3.46	4.48	3.39	2.59	3.45
0.75	3.45	2.49	3.58	4.64	3.51	2.78	3.57
1	3.54	2.61	3.67	4.75	3.60	2.91	3.66
2	3.74	2.83	3.89	5.03	3.81	3.15	3.87
5	4.08	2.95	4.24	5.48	4.15	3.29	4.22
10	4.44	3.03	4.61	5.97	4.52	3.37	4.60
15	4.66	3.08	4.84	6.27	4.74	3.43	4.82
20	4.81	3.11	4.99	6.46	4.89	3.47	4.97
∞	2.92	3.32	3.03	3.92	2.97	3.70	3.02

ed edges allow rotation, contributing to more considerable deflections than the clamped conditions. The effect of free edge in maximizing the deflections is more evident when the results are compared with SSSS boundary condition.

The smallest maximum deflection values are obtained in the case of CCCC. They are very close to results obtained from CCSS, CCCF, and CCFF, which indicates the effect of clamped boundary conditions in minimizing the deflections in FGM plates. In the case of CSCS, although it also has two clamped and two simply supported edges like CCSS, the positions of the clamped edges can affect the deflection values. In CSCS, the two clamped edges are adjacent, while in CCSS, the clamped edges are opposed. It is also worth mentioning that in CCSS boundary conditions, one of the clamped edges is longer than the clamped edges in CSCS, which makes the plate more constrained, decreasing deflections. Maximum 1st principle stresses of FGM plates are presented similarly in Tables 8–10 and are compared in Figures 9–11.

As can be observed in Figures 9–11, FGM plates with SSSS boundary conditions have the lowest values of maximum 1st principle stress under both distributed loads. In contrast, the case of concentrated point load has the highest values after SSSF. This is because of the localized nature of the point load, which adds steepness to the trends in lower values of n and causes an overall increase in stress values compared to both distributed loads. Results corresponding to CCCF and CCFF boundary conditions are very close to each other in the case of uniformly distributed and concentrated point loads. By observing all three figures, it is apparent that the trends of stress values for CCCC, CCSS, CCCF, and CCFF boundary conditions converged as the load type changed from uniformly to sinusoidal distributed load and then to concentrated point load. This indicates that the two clamped edges take most of the stress. CSCS boundary condition exhibited the highest results of 1st principle stress in the plates under both distributed loads but had lower stress values than SSSF and SSSS in the case of concentrated point load.

Table 10. Maximum 1st principle stresses (MPa) of isotropic homogeneous and FGM rectangular plates under concentrated point load

Power-law index (n)	Boundary conditions						
	CCCC	SSSS	CCSS	CSCS	CCCF	SSSF	CCFF
0	37.5	43.5	37.6	39.3	37.5	44.2	37.6
0.1	21.5	25.0	21.5	22.5	21.5	25.4	21.6
0.25	23.5	27.4	23.6	24.7	23.6	27.8	23.6
0.5	26.2	30.5	26.3	27.5	26.3	31.0	26.3
0.75	28.1	32.7	28.2	29.5	28.2	33.2	28.2
1	29.5	34.3	29.6	30.9	29.5	34.8	29.6
2	31.9	37.1	32.0	33.5	32.0	37.7	32.0
5	33.3	38.8	33.4	35.0	33.4	39.4	33.4
10	34.2	39.7	34.3	35.9	34.2	40.3	34.3
15	34.8	40.4	34.9	36.5	34.8	41.0	34.9
20	35.2	40.9	35.3	36.9	35.2	41.5	35.3
∞	37.5	43.5	37.6	39.3	37.5	44.2	37.6

Table 11. Maximum Von Mises stresses (MPa) of isotropic homogeneous and FGM rectangular plates under uniformly distributed load

Power-law index (n)	Boundary conditions						
	CCCC	SSSS	CCSS	CSCS	CCCF	SSSF	CCFF
0	3.80	6.51	4.00	5.31	4.39	7.02	4.37
0.1	3.95	6.78	4.16	5.53	4.57	7.30	4.55
0.25	4.12	7.08	4.34	5.77	4.77	7.62	4.75
0.5	4.34	7.45	4.57	6.07	5.02	8.03	5.01
0.75	4.49	7.71	4.74	6.29	5.20	8.31	5.18
1	4.61	7.90	4.85	6.44	5.33	8.52	5.31
2	4.87	8.34	5.13	6.81	5.63	9.01	5.61
5	5.31	9.08	5.60	7.43	6.12	9.83	6.11
10	5.78	9.89	6.10	8.09	6.67	10.7	6.65
15	6.07	10.4	6.40	8.49	7.00	11.2	6.98
20	6.26	10.7	6.60	8.76	7.22	11.6	7.20
∞	3.80	6.51	4.00	5.31	4.39	7.02	4.37

Table 12. Maximum Von Mises stresses (MPa) of isotropic homogeneous and FGM rectangular plates under sinusoidal distributed load

Power-law index (n)	Boundary conditions						
	CCCC	SSSS	CCSS	CSCS	CCCF	SSSF	CCFF
0	2.59	3.44	2.69	3.48	2.64	3.59	2.68
0.1	2.70	3.58	2.80	3.62	2.47	3.74	2.79
0.25	2.81	3.74	2.92	3.78	2.86	3.90	2.91
0.5	2.96	3.94	3.08	3.98	3.01	4.11	3.07
0.75	3.07	4.08	3.19	4.12	3.12	4.26	3.17
1	3.14	4.18	3.27	4.22	3.20	4.36	3.25
2	3.33	4.41	3.45	4.47	3.38	4.60	3.44
5	3.63	4.80	3.77	4.87	3.69	5.01	3.75
10	3.95	5.23	4.10	5.30	4.02	5.45	4.08
15	4.14	5.49	4.30	5.57	4.22	5.73	4.29
20	4.27	5.66	4.44	5.74	4.35	5.91	4.42
∞	2.59	3.44	2.69	3.48	2.64	3.59	2.68

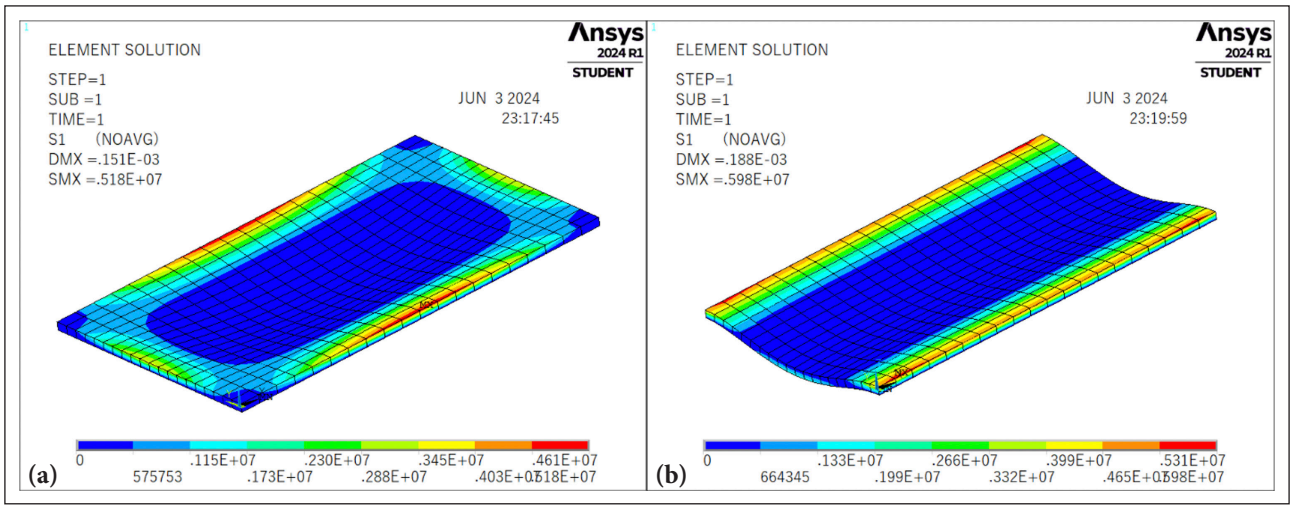

Figure 12. 1st Principle stresses in FGM rectangular plates with (a) CCCC and (b) CCFF boundary conditions.

Table 13. Maximum Von Mises stresses (MPa) of isotropic homogeneous and FGM rectangular plates under concentrated point load

Power-law index (n)	Boundary conditions						
	CCCC	SSSS	CCSS	CSCS	CCCF	SSSF	CCFF
0	35.6	41.1	35.6	37.3	35.6	41.4	35.6
0.1	37.0	42.8	37.0	38.8	37.0	43.1	37.0
0.25	38.6	44.6	38.7	40.5	38.6	44.9	38.7
0.5	40.7	47.0	40.7	42.7	40.7	47.3	40.7
0.75	42.1	48.7	42.2	44.2	42.1	49.0	42.1
1	43.2	49.9	43.2	45.3	43.2	50.2	43.2
2	45.7	52.8	45.7	47.9	45.7	53.2	45.7
5	49.8	57.6	49.9	52.3	49.8	58.0	49.9
10	54.2	62.7	54.3	56.9	54.2	63.1	54.3
15	56.9	65.8	57.0	59.7	56.9	66.2	56.9
20	58.7	67.8	58.7	61.5	58.7	68.3	58.7
∞	35.6	41.1	35.6	37.3	35.6	41.4	35.6

Moreover, the trends show an increase in stress values for all boundary conditions as the power-law index increases. This is a result of the transition of materials from alumina to steel, affecting the stiffness of the plate. At higher values of n, the ductile nature of steel decreases the steepness of the trends. Figure 12 shows the formation of 1st principle stresses in the FGM plates (n=1) subjected to uniformly distributed load with CCCC and CCFF boundary conditions.

Maximum Von Mises stresses of the FGM rectangular plates with different boundary conditions for all three types of loads are tabulated in Tables 11–13 and are compared in Figures 13–15.

As can be seen in Figures 10–12, FGM plates with SSSF and SSSS boundary conditions have higher maximum Von Mises stress values under all types of loads compared to other boundary conditions, except plates subjected to sinusoidal distributed load, where stress values of CSCS boundary condition surpassed those of SSSS. In the case of CCCF and CCFF, when the plates are subjected to uniformly distributed load, there is a very small difference in stress values, and their trends are nearly coincident. Under sinusoidal distributed load, these trends diverged enough to be observed. The maximum Von Mises stress values for FGM plates subjected to concentrate point load with CCCC,

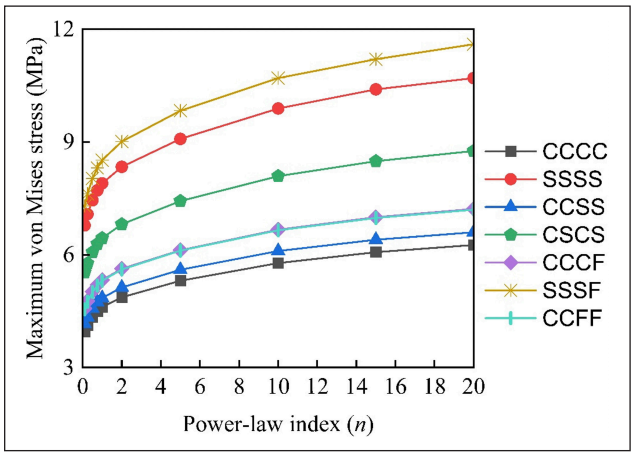

Figure 13. Maximum Von Mises stresses of FGM rectangular plates under uniformly distributed load.

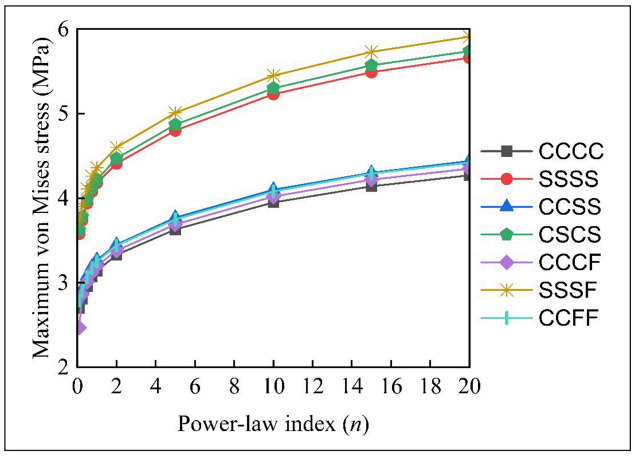

Figure 14. Maximum Von Mises stresses of FGM rectangular plates under sinusoidal distributed load.

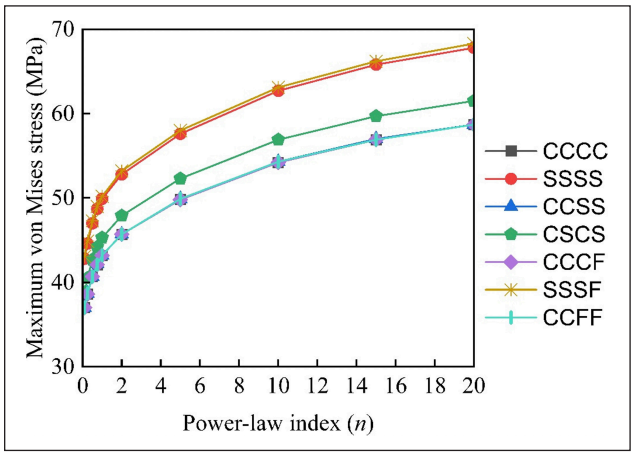

Figure 15. Maximum Von Mises stresses of FGM rectangular plates under concentrated point load.

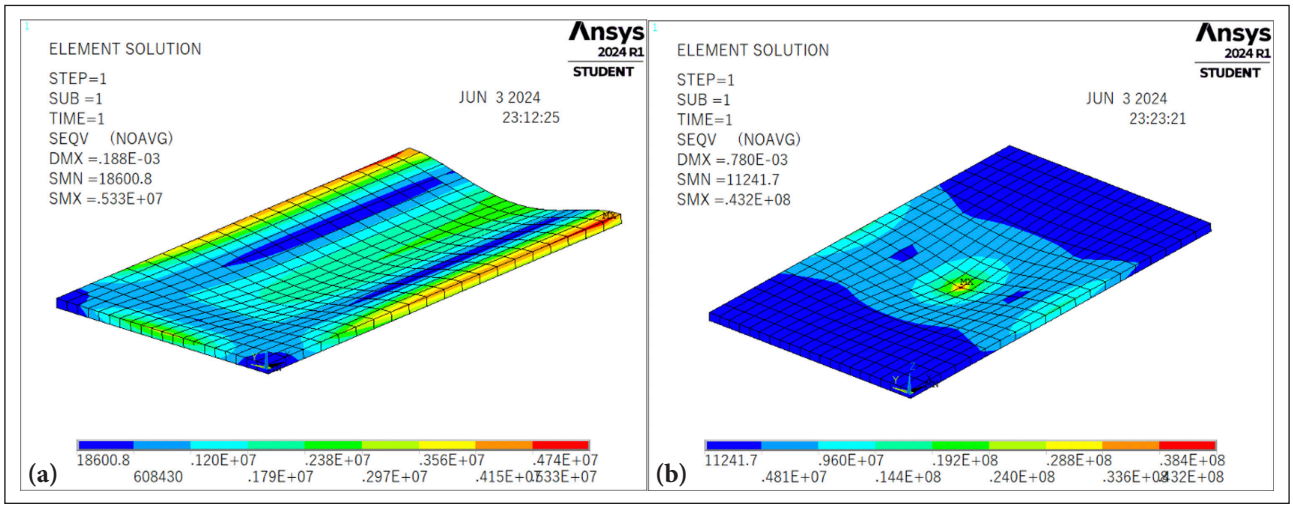

Figure 16. Von Mises stresses in FGM rectangular plates; **(a)** Subjected to uniformly distributed load with CCCF boundary condition **(b)** Subjected to concentrated point load with CCCC boundary condition.

CCSS, CCCF, and CCFF are very close and have small differences that can be neglected. The common factor between these four boundary conditions is the presence of clamped supports at the two long edges of the plate. CSCS boundary conditions also have two clamped edges, but one of them is the short edge of the plate, resulting in higher stress values than others. This indicates the clamped boundary condition's significance and position around the plate. In the case of point load, the maximum Von Mises stress values corresponding to SSSF and SSSS were very close at small values of n, but the trends diverged smoothly at greater values of n. Across all load types, the power-law index n influenced the maximum Von Mises stress values similarly, with an initial increase due to higher deflections from introducing steel-like properties. At higher n values, the rate of increase in stress values decreased as the plate gained more ductility due to the high content of steel in the composition. Figure 16 shows the formation of Von Mises stresses in FGM rectangular plates (n=1) subjected to uniformly distributed load with CCCF boundary condition and concentrated point load with CCCC boundary condition.

4. CONCLUSIONS

This paper investigates the effect of the material property gradient on the deflection and stress responses of FGM plates with various boundary conditions, subjected to three different types of loads, using the finite element method. Ten FGM plates, whose top and bottom layers are composed of alumina and steel, respectively, have intermediate layers with material properties varying based on the power-law indexes considered in this study. After obtaining numerical results from ANSYS Mechanical APDL and comparing them, the following conclusions can be drawn:

- The number of layers and mesh size significantly influence the actual behavior of FGM plates. While an increase in the number of layers and mesh size leads to more precise and accurate numerical results, no significant change in results was observed when the number of layers increased from 101 to 201 or when the mesh size was refined beyond 20 x 20.
- The type of load plays a crucial role in determining the deflections and stress formation within the FGM plates.

A sinusoidally distributed load resulted in the least deflections and stress values compared to uniformly distributed and concentrated point loads.

- Boundary conditions have a significant impact on deflections in FGM plates. Under all types of loads, plates with CCCC (all clamped) boundary conditions exhibited the least maximum deflection, while plates with SSSF (three simply supported, one free) boundary conditions showed the highest maximum deflection.
- The highest values of maximum first principal stress were observed in plates with CSCS (clamped-simply supported-clamped-simply supported) boundary conditions when subjected to distributed loads. These highest values shifted to plates with SSSF boundary conditions under concentrated point loads. In the case of distributed loads, the lowest stress was recorded in plates with SSSS (all simply supported) boundary conditions, while the lowest values under concentrated point loads were seen in plates with CCCC boundary conditions.
- For all types of loads, the highest maximum von Mises stress values in all FGM plates were recorded under SSSF boundary conditions. The lowest maximum von Mises stress values were observed in plates with CCCC boundary conditions when subjected to uniformly distributed and concentrated point loads. Under sinusoidal distributed loads, the lowest stress value was observed in plates with CCCF (three clamped, one free) boundary conditions.
- The positioning of clamped edges greatly influences the deflections and stress formation within FGM plates.
- Generally, increasing the steel content in the composition of the plates, thereby increasing the power-law index (n), resulted in higher deflections and maximum first principal and von Mises stresses in all the plates.
- At smaller values of n, the rate of increase in deflections, maximum first principal stress, and von Mises stress is higher than at larger values of n, where the plates exhibit more steel-like properties.

The results of this study are in strong agreement with the existing literature consensus, emphasizing the impact of the material gradient index and boundary conditions on the bending and stress responses of FGM plates.

ETHICS

There are no ethical issues with the publication of this manuscript.

DATA AVAILABILITY STATEMENT

The authors confirm that the data that supports the findings of this study are available within the article. Raw data that support the finding of this study are available from the corresponding author, upon reasonable request.

CONFLICT OF INTEREST

The authors declare that they have no conflict of interest.

FINANCIAL DISCLOSURE

The authors declared that this study has received no financial support.

USE OF AI FOR WRITING ASSISTANCE

Not declared.

PEER-REVIEW

Externally peer-reviewed.

REFERENCES

[1] Zhang, N., Khan, T., Guo, H., Shi, S., Zhong, W., & Zhang, W. (2019). Functionally graded materials: An overview of stability, buckling, and free vibration analysis. *Adv Mater Sci Eng, 2019*(1), 1354150. [CrossRef]

[2] Edwin, A., Anand, V., & Prasanna, K. (2017). Sustainable development through functionally graded materials: An overview. *Rasayan J Chem, 10*(1), 149–152.

[3] Torelli, G., Fernández, M. G., & Lees, J. M. (2020). Functionally graded concrete: Design objectives, production techniques and analysis methods for layered and continuously graded elements. *Constr Build Mater, 242*, 118040. [CrossRef]

[4] Chan, R., Hu, T., Liu, X., Galobardes, I., Moy, C. K., Hao, J. L., & Krabbenhoft, K. (2019). Sustainability analysis of functionally graded concrete produced with fibres and recycled aggregates. *In Sustainable Buildings and Structures: Building a Sustainable Tomorrow* (pp. 38–44). CRC Press. [CrossRef]

[5] Shamoon, A., Haleem, A., Bahl, S., Javaid, M., Prakash, C., & Budhhi, D. (2022). Understanding the role of advanced materials for energy infrastructure and transmission. *Mater Today Proc, 62*, 4260–4266. [CrossRef]

[6] Koizumi, M., & Niino, M. (1995). Overview of FGM research in Japan. *MRS Bull, 20*(1), 19–21. [CrossRef]

[7] Sobczak, J., & Drenchev, L. (2008). Functionally graded materials - Processing and modeling. *Motor Transport Inst Warsaw Foundry Res Inst*, Cracow.

[8] Chaabani, H., Mesmoudi, S., Boutahar, L., & El Bikri, K. (2023). A high-order finite element continuation for buckling analysis of porous FGM plates. *Eng Struct, 279*, 115597. [CrossRef]

[9] Moita, J. S., Correia, V. F., Soares, C. M. M., & Herskovits, J. (2019). Higher-order finite element models for the static linear and nonlinear behaviour of functionally graded material plate-shell structures. *Compos Struct, 212*, 465–475. [CrossRef]

[10] Afzali, M., Farrokh, M., & Carrera, E. (2022). Thermal buckling loads of rectangular FG plates with temperature-dependent properties using Carrera unified formulation. *Compos Struct, 295*, 115787. [CrossRef]

[11] Kazemzadeh-Parsi, M. J., Ammar, A., & Chinesta, F. (2023). Parametric analysis of thick FGM plates based on 3D thermo-elasticity theory: A proper generalized decomposition approach. *Mater, 16*(4), 1753. [CrossRef]

[12] Kargarnovin, M. H., Pouladvand, M., & Najafizadeh, M. M. (2023). Study of thermal stability of thin rectangular plates with variable thickness made of functionally graded materials. *J Mech Res Appl, 13*(3), 1–28.

[13] Saad, M., & Hadji, L. (2022). Thermal buckling analysis of porous FGM plates. *Mater Today Proc, 53*, 196–201. [CrossRef]

[14] Slimani, R., Menasria, A., Ali Rachedi, M., Mourad, C., Refrafi, S., Nimer, A. A., & Mamen, B. (2024). A novel quasi-3D refined HSDT for static bending analysis of porous functionally graded plates. *J Comput Appl Mech, 55*(3): 519–537.

[15] Rebai, B., Mansouri, K., Chitour, M., Berkia, A., Messas, T., Khadraoui, F., & Litouche, B. (2023). Effect of idealization models on deflection of functionally graded material (FGM) plate. *J Nano Electron Phys, 15*(1), 01022. [CrossRef]

[16] Hamza Madjid, B., & Bouderba, B. (2023). Buckling analysis of FGM plate exposed to different loads conditions. *Mech Based Des Struct Mach, 51*(12), 6798–6813. [CrossRef]

[17] Hong, N. T. (2020). Nonlinear static bending and free vibration analysis of bidirectional functionally graded material plates. *Int J Aerosp Eng, 2020*, 1–16. [CrossRef]

[18] Talha, M., & Singh, B. (2010). Static response and free vibration analysis of FGM plates using higher order shear deformation theory. *Appl Math Model, 34*(12), 3991–4011. [CrossRef]

[19] Singh, D., & Gupta, A. (2024). Influence of microstructural defects on vibration characteristics of sandwich double FGM layer under mixed boundary conditions. *Int J Interact Des Manuf, 2024*, 1–18. [CrossRef]

[20] Alghanmi, R. A., & Aljaghthami, R. H. (2024). A four-variable shear deformation theory for the static analysis of FG sandwich plates with different porosity models. *Math Comput Appl, 29*(2), 20. [CrossRef]

[21] Nguyen, T. T., Le, T. S., Tran, T. T., & Pham, Q. H. (2024). Buckling analysis of functionally graded porous variable thickness plates resting on Pasternak foundation using ES-MITC3. *Lat Am J Solids Struct, 21*, e524. [CrossRef]

[22] Elkafrawy, M., Alashkar, A., Hawileh, R., & AlHamaydeh, M. (2022). FEA investigation of elastic buckling for functionally graded material (FGM) thin plates with different hole shapes under uniaxial loading. *Buildings, 12*(6), 802. [CrossRef]

[23] Alashkar, A., Elkafrawy, M., Hawileh, R., & AlHamaydeh, M. (2022). Buckling analysis of functionally graded materials (FGM) thin plates with various circular cutout arrangements. *J Compos Sci, 6*(9), 277. [CrossRef]

[24] Alashkar, A., Elkafrawy, M., Hawileh, R., & AlHamaydeh, M. (2024). Elastic buckling behaviour of skew functionally graded material (FGM) thin plates with circular openings. *Buildings, 14*(3), 572. [CrossRef]

[25] Kumar, R., Sharma, H. K., Gupta, S., Malguri, A., Rajak, B., Srivastava, Y., & Pandey, A. (2024). Initial buckling behavior of elastically supported rectangular FGM plate based on higher order shear deformation theory via spline RBF method. *Mech Adv Compos Struct, 11*(1), 59–72.

[26] Shehab, M. B., Taima, M. S., Sayed, H., & El-Sayed, T. A. (2023). An investigation into the free vibration of intact and cracked FGM plates. *J Fail Anal Prev, 23*(5), 2142–2168. [CrossRef]

[27] Hu, Z., Shi, Y., Xiong, S., Zheng, X., & Li, R. (2023). New analytic free vibration solutions of non-Lévy-type porous FGM rectangular plates within the symplectic framework. *Thin-Walled Struct, 185*, 110609. [CrossRef]

[28] Peng, L. X., Chen, S. Y., Wei, D. Y., Chen, W., & Zhang, Y. S. (2022). Static and free vibration analysis of stiffened FGM plate on elastic foundation based on physical neutral surface and MK method. *Compos Struct, 290*, 115482. [CrossRef]

[29] Lim, J., Amir, M., Kim, S. W., & Lee, S. Y. (2024). Static analysis of FGM porous cooling plates with cutouts: A multilayered approach. *Adv Compos Mater, 2024*(2303947), 1–24. [CrossRef]

[30] Ramu, I., & Mohanty, S. C. (2014). Modal analysis of functionally graded material plates using finite element method. *Procedia Mater Sci, 6*, 460–467. [CrossRef]

[31] Srivastava, M. C., & Singh, J. (2023). Assessment of RBFs based meshfree method for the vibration response of FGM rectangular plate using HSDT model. *Mech Adv Compos Struct, 10*(1), 137–150.

[32] Kumar, Y. (2022). Effect of elastically restrained edges on free transverse vibration of functionally graded porous rectangular plate. *Mech Adv Compos Struct, 9*(2), 335–348.

[33] Kumaravelan, R. *Thermo mechanical analysis of functionally graded material plates* [Thesis, Anna University].

[34] Smaine, A., Mokhtari, M., Telli, F., Khiari, M. E. A., Bouchetara, M., & Habib, B. (2024). Using FGM concept in fiber-matrix coupling laws to predict the damage in carbon-epoxy graded composite application in notched plate under thermo-mechanical loading. *Mech Adv Mater Struct*, 1–15. [CrossRef]

[35] Asemi, K., & Salami, S. J. (2015). A study on low velocity impact response of FGM rectangular plates with 3D elasticity based graded finite element modeling. *J Theor Appl Mech, 53*(4), 859–872. [CrossRef]

[36] Rani, P., Verma, D., & Ghangas, G. (2023). Modeling and stress analysis of rounded rectangular inclusion enclosed by FGM layer. *Int J Math Eng Manag Sci, 8*(2), 282. [CrossRef]

[37] Yildirim, S. (2020). Hydrogen elasticity solution of functionally-graded spheres, cylinders and disks. *Int J Hydrogen Energy, 45*(41), 22094–22101. [CrossRef]

[38] Feri, M., Krommer, M., & Alibeigloo, A. (2023). Three-dimensional static analysis of a viscoelastic rectangular functionally graded material plate embedded between piezoelectric sensor and actuator layers. *Mech Based Des Struct Mach, 51*(7), 3843–3867. [CrossRef]

[39] Bendenia, N., Zidour, M., Bousahla, A. A., Bourada, F., Tounsi, A., Benrahou, K. H., & Tounsi, A. (2020). Deflections, stresses and free vibration studies of FG-CNT reinforced sandwich plates resting on Pasternak elastic foundation. *Comput Concr Int J, 26*(3), 213–226.

[40] Noori, A. R., Aslan, T. A., & Temel, B. (2018). An efficient approach for in-plane free and forced vibrations of axially functionally graded parabolic arches with nonuniform cross section. *Compos Struct, 200*, 701–710. [CrossRef]

[41] Noori, A. R., Aslan, T. A., & Temel, B. (2021). Dynamic analysis of functionally graded porous beams using complementary functions method in the Laplace domain. *Compos Struct, 256*, 113094. [CrossRef]

[42] Aslan, T. A., Noori, A. R., & Temel, B. (2023, December). An efficient approach for free vibration analysis of functionally graded sandwich beams of variable cross-section. *In Struct* (Vol. 58, p. 105397). Elsevier. [CrossRef]

[43] Doori, S. G. M., Noori, A. R., & Etemadi, A. (2024). Static response of functionally graded porous circular plates via finite element method. *Arab J Sci Eng, 49*, 14167–14181. [CrossRef]

[44] Özer, A. P., Noori, A. R., & Aygörmez, Y. (2023, November 23-25). *Effect of mesh size on finite element analysis of functionally graded porous domes*. International Conference on Engineering Technologies (ICENTE23), Konya, Türkiye.

[45] Al-ıtbı, S. K., & Noori, A. R. (2022). Influence of porosity on the free vibration response of sandwich functionally graded porous beams. *J Sustain Constr Mater Technol, 7*(4), 291–301. [CrossRef]

[46] Lee, J. K., & Lee, B. K. (2019). Free vibration and buckling of tapered columns made of axially functionally graded materials. *Appl Math Model, 75*, 73–87. [CrossRef]

[47] Huang, Y., & Li, X. F. (2010). Buckling of functionally graded circular columns including shear deformation. *Mater Des, 31*(7), 3159–3166. [CrossRef]

[48] Yildirim, S. (2020). Free vibration analysis of sandwich beams with functionally-graded-cores by complementary functions method. *AIAA J, 58*(12), 5431–5439. [CrossRef]

[49] Menasria, A., Kaci, A., Bousahla, A. A., Bourada, F., Tounsi, A., Benrahou, K. H., & Mahmoud, S. R. (2020). A four-unknown refined plate theory for dynamic analysis of FG-sandwich plates under various boundary conditions. *Steel Compos Struct Int J, 36*(3), 355–367.

[50] Rabhi, M., Benrahou, K. H., Kaci, A., Houari, M. S. A., Bourada, F., Bousahla, A. A., & Tounsi, A. (2020). A new innovative 3-unknowns HSDT for buckling and free vibration of exponentially graded sandwich plates resting on elastic foundations under various boundary conditions. *Geomech Eng, 22*(2), 119–132.

[51] Matouk, H., Bousahla, A. A., Heireche, H., Bourada, F., Bedia, E. A., Tounsi, A., & Benrahou, K. H. (2020). Investigation on hygro-thermal vibration of P-FG and symmetric S-FG nanobeam using integral Timoshenko beam theory. *Adv Nano Res, 8*(4), 293–305.

[52] Hassan, A. H. A., & Kurgan, N. (2019). Modeling and buckling analysis of rectangular plates in ansys. *Int J Eng Appl Sci, 11*(1), 310–329. [CrossRef]

[53] Liu, Y., & Glass, G. (2013, April 16-18). *Effects of mesh density on finite element analysis*. SAE Tech Pap, Detroit, USA. [CrossRef]

[54] More, S. T., & Bindu, R. S. (2015). Effect of mesh size on finite element analysis of plate structure. *Int J Eng Sci Innov Technol, 4*(3), 181–185.

[55] ANSYS Inc. (2024). Gain greater engineering and product life cycle perspectives: 2024 product releases & updates. *ANSYS 2024 R1*. Canonsburg, PA. https://www.ansys.com/products/release-highlights

[56] Singha, M. K., Prakash, T., & Ganapathi, M. (2011). Finite element analysis of functionally graded plates under transverse load. *Finite Elem Anal Des, 47*(4), 453–460. [CrossRef]

[57] Delale, F., & Erdogan, F. (1983). The crack problem for a nonhomogeneous plane. *ASME J Appl Mech, 50*(3), 609–614. [CrossRef]

[58] ANSYS Mechanical APDL Element Reference. (2013). *Mechanical APDL element reference*. Pennsylvania: ANSYS Inc.